Indian Journal of Chemical Technology
Vol. 27, May 2020, pp. 235-242

Preparation of a CeO_2/γ-Al_2O_3 composite and its catalytic degradation performance

Youfeng Li*,[1], Jingliang Lin [1], Guangwei Wang[1] & Guoqing Liu [2]
[1]School of Chemistry and Chemical Engineering, Zunyi Normal College, Zunyi, 563006, China
[2]School of Chemistry and Chemical Engineering, Hunan University of Science and Technology, Xiangtan 411201, China
Email: liyoufeng2005@sina.com

Received 16 February 2019; accepted 17 February 2020

CeO_2/γ-Al_2O_3 composite catalyst has been prepared using CeO_2 as an active component and γ-Al_2O_3 as a support to remove dye from wastewater by catalytic degradation. The catalytic performance of the CeO_2/γ-Al_2O_3 sample for the degradation of methylene blue is studied under visible light irradiation. The results show the presence of γ-Al_2O_3 and CeO_2 with a cubic fluorite structure in the CeO_2/γ-Al_2O_3 samples synthesized at 550°C. Small CeO_2/γ-Al_2O_3 particle and a good dispersion of CeO_2 are achieved with loading of CeO_2. The loading of CeO_2 on γ-Al_2O_3 also increases the total pore volume and pore diameter, which results in a high specific surface area of 132.03 m^2/g, a total pore volume of 0.74 cm^3/g, and a mean pore diameter of 22.54 nm. The photocatalytic degradation efficiency of methylene blue by the CeO_2/γ-Al_2O_3 catalyst is higher than those of CeO_2 and γ-Al_2O_3. Under the same conditions the CeO_2/γ-Al_2O_3 catalyst achieves 98.36% degradation at 80 min, higher 5.0% and 11.9% degradation than CeO_2 and γ-Al_2O_3, respectively. The high efficiency is attributed to promotion of the structural and textural performance of the CeO_2/γ-Al_2O_3 catalyst by synergistic interaction between CeO_2 and γ-Al_2O_3. These performances promote a larger surface area, higher content of acid sites, more •OH radicals and higher redox properties of the catalyst. The catalytic reaction kinetics could be fitted by the heterogeneous Langmuir-Hinshelwood model and the pseudo-first order rated constant for k_{app} is 17.5×10^{-2}, which is 1.33 and 2.5 times as big as those of CeO_2 and γ-Al_2O_3, respectively. CeO_2/γ-Al_2O_3 catalyst suggests promising application for practical dye pollutant treatment.

Keywords: Composite catalyst, CeO_2/γ-Al_2O_3, Methylene blue, Catalytic degradation, Wastewater treatment

Wastewater from textile dying contains many organic pollutants that can cause considerable damage to the environment and human health[1,2]. These highly stable organic pollutions in wastewater can be treated by different techniques, such as adsorption, catalytic wet oxidation and photocatalysis[3-5]. Photocatalysis techniques are considered to be a promising method for destroying these organic pollutions because of the low amounts of secondary pollution produced simple operation, and mild reaction conditions[6]. Photocatalysis is based on redox reactions that occur when a semiconductor material is irradiated by light. Ceria oxide (CeO_2) has a high oxygen storage capacity and the ability to release or take up oxygen under ultraviolet irradiation owing to the Ce^{4+}/Ce^{3+} redox couple, making it a useful photocatalyst for degradation processes[7,8]. Many methods have been developed to design and synthesize CeO_2 photocatalyst aimed at providing improved photocatalytic performance[9-11].

Depositing ceria onto materials with large surface areas has been reported to promote the activity of the catalyst. Large surface areas ensure greater contact sites between the catalytic phase and the treated wastewater. Carbon nanotubes are often used as a catalyst support owing to their high surface areas. Peng et al prepared ceria nanoparticles supported on carbon nanotubes (CeO_2-CNTs) for the removal of arsenate from water[12]. Their experimental results showed that CeO_2-CNTs are an effective adsorbent for arsenate in the purification of drinking water. Catalytic performance of CeO_2 can be enhanced by confining CeO_2 inside carbon nanotubes for dehydrogenation of ethylbenzene owing to the synergistic effects between the CeO_2 and carbon nanotubes[13]. Phanichphant *et al*. applied CeO_2/SiO_2 to photodegradation of rhodamine B and discovered that a CeO_2/SiO_2 supported catalyst showed greater degradation efficiency than that of pure ceria under visible light irradiation[14]. The effects of depositing CeO_2 onto Fe_2O_3/γ-Al_2O_3 catalysts for catalytic wet peroxide oxidation of azo dyes have also been studied. The results have shown that Fe_2O_3/γ-Al_2O_3 and Fe_2O_3-CeO_2/γ-Al_2O_3 are suitable catalysts for degradation of contaminants at normal temperatures and atmospheric pressure [15].

γ-Al_2O_3 is widely used as a catalyst support and adsorbent owing to its high oxide content and large surface area. Ceria deposited on alumina is an important catalyst in redox reactions. Neves et al [16] investigated the effectiveness of CeO_2/Al_2O_3 as a photocatalyst for dye degradation when a sample with 24wt% CeO_2 loaded on Al_2O_3 showed the highest activity at neutral *p*H for methylene blue photodegradation and 93% dye degradation was achieved. This composite was more cost effective than pure ceria. However, further research is needed to improve the photocatalytic performance and explain the mechanism of the degradation process. In this work, we prepared CeO_2/γ-Al_2O_3 nanocomposite catalysts loaded with CeO_2 as an active component and γ-Al_2O_3 as a carrier to improve catalytic degradation efficiency of methylene blue in dye wastewater. The structure and catalytic performance of CeO_2/γ-Al_2O_3 samples was investigated by X-ray diffraction (XRD), transmission electron microscopy (TEM), Brunauer-Emmett-Teller (BET) surface area analysis, NH_3-Temperature Programmed Desorption (TPD), X-ray photoelectron spectroscopy (XPS) and UV-Visible spectrophotometer. Thus, we present a new synthesis of ceria loaded onto alumina for application of catalysis and develop an understanding of the catalytic degradation mechanism.

Experimental Section

Preparation of CeO_2/γ-Al_2O_3 catalyst

The reagents $Ce(NO_3)_3$•$6H_2O$, NH_4HCO_3, polyethyleneglycol (PEG) and methylene blue were of analytical grade. Deionized water was used in all experiments. The γ-Al_2O_3 powder was made from carbonating sodium aluminate solution in our laboratory.

CeO_2 samples were prepared by a precipitation method, with the use of polyethyleneglycol (PEG) as a dispersant dissolved in nitrate precursor $Ce(NO_3)_3$•$6H_2O$ solution. The precipitator NH_4HCO_3 was added into to $Ce(NO_3)_3$•$6H_2O$ solution to aid precipitation at 80°C under agitation. After aging at room temperature for 24 h, the precipitate was filtrated and washed with deionized water. The CeO_2 samples were obtained after the precipitate being dried at 100°C for 10 h, followed by calcination in a muffle furnace at 550°C for 4 h. The CeO_2/γ-Al_2O_3 catalyst was prepared by an impregnation method in which CeO_2 was used as the active component and γ-Al_2O_3 as a support. The mole ratio of CeO_2 to γ-Al_2O_3 was controlled to be in the range of 0–0.07. The CeO_2/γ-Al_2O_3 catalyst was obtained by impregnation of 2 g γ-Al_2O_3 with 100 mL aqueous solution containing stoichiometric CeO_2 for 2 h under magnetic stirring at room temperature. The samples were then dried at 80°C for 12 h. The dried samples were calcined at 550°C in a muffle furnace for 3 h to obtain the CeO_2/γ-Al_2O_3 catalyst.

Catalytic degradation experiments

Catalytic degradation experiments were performed in a double beaker of 250 mL with water cooling. A portion of catalyst (5–20 mg) and H_2O_2 (6 mL) were introduced into 100 mL of aqueous dye solution containing methylene blue at a concentration of 100 mg/L. Sodium hydroxide was used to adjust the *p*H of the solution. Adsorption equilibrium was attained by the reaction solution after magnetic stirring for 30 min in the dark. The degradation reaction was then performed using 300 W Xenon lamps as visible light. Liquid samples were removed at regular 20 min intervals for analysis of the absorbance. To evaluate the catalytic activity of the catalysts, the dye removal efficiency (η) was calculated, as shown below:

$$\eta = \frac{c_0 - c_t}{c_0} \times 100\%$$

where c_0 and c_t are the initial and different times absorbance values of methylene blue, respectively.

Catalyst characterization

The crystalline phases of the as-prepared composite oxides were studied by x-ray diffraction (XRD) with a Bruker/AXS D8 Advance X-ray diffractometer operated at 40 kV and 200 mA with Cu Ka radiation (λ = 0.15418 nm). The morphology and dispersion of the powders were observed with the use of a transmissionelectron microscope (TEM, JEOL-6360LV). Textural properties of the samples were measured by the BET model on a Quantachrome NOVA instrument, with Aras the carrier gas and N_2 as the adsorbent at −196°C. The surface acidity of the catalyst was measured by NH_3-TPD using 100 mg samples heated at 10°/min to 500°C, and then decreased to room temperature after 60 min. Adsorbed ammonia for 30 min, then heated to 700°C and desorbed, Surface acidity of the sample area was compared by the peak area of desorption curve. XPS was performed to analyze the surface element valence

states of the catalysts with a PHI5700 analyzer with an Al-Ka X-ray source at 250 W and 12.5 kV. The visible light absorbance at the characteristic wavelength of 664 nm for methylene blue dye was measured with an UV-2500 spectrophotometer.

Results and Discussion

Crystal structure analysis

The XRD results of the γ-Al_2O_3, CeO_2, and CeO_2/γ-Al_2O_3 catalyst samples are shown in Fig. 1. The mole ratio of Ce loaded onto the CeO_2/γ-Al_2O_3 catalyst was 0.03 (denoted as 3%CeO_2/γ-Al_2O_3). Characteristic peaks of the γ-Al_2O_3 phase were apparent at 2θ =33.1°, 36.0°, 46.1°, and 67.0°. Clear diffraction peaks were observed at 2θ = 28.5°, 33.0°, 47.5°, 59.0°, 69.5°, and 79.0°, in agreement with the (111), (200), (220), (311), (400), and (422) planes of the cubic fluorite structure of CeO_2, respectively. Some γ-Al_2O_3 and CeO_2 characteristic peaks were also observed in the XRD patterns for the CeO_2/γ-Al_2O_3 samples. These results showed that the main active component of the catalyst was CeO_2 crystallized with a cubic fluorite structure and this structure remained after the calcination process. However, the peak intensities of the CeO_2/γ-Al_2O_3 sample became weaker compared with those of the CeO_2 and γ-Al_2O_3 samples. This finding suggested a good dispersion of CeO_2 particles on the γ-Al_2O_3 support with CeO_2/γ-Al_2O_3 catalyst particles of an overall small size.

Sample morphology analysis

TEM imaging was used to investigate the morphology of the samples. Fig. 2 shows TEM images of the γ-Al_2O_3, CeO_2, and 3%CeO_2/γ-Al_2O_3 samples. Flake-like 10-nm structures were found for the γ-Al_2O_3 samples and CeO_2 featured a columnar morphology with widths of approximately 50 nm, as observed in Fig. 2. The loading of CeO_2 particles on the surface of the CeO_2/γ-Al_2O_3 catalyst is shown in Fig. 2(c). A better dispersion of the γ-Al_2O_3 particles was achieved by loading of CeO_2, where the columnar structure of CeO_2 was broken.

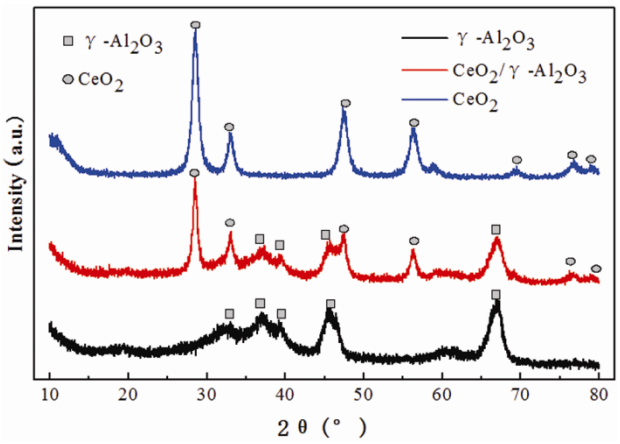

Fig. 1 — XRD patterns of the catalyst samples.

BET surface area analysis

The BET surface area, total pore volume, and average pore size of the γ-Al_2O_3, CeO_2, and 3%CeO_2/γ-Al_2O_3 samples are listed in Table 1. The CeO_2/γ-Al_2O_3 catalyst sample featured a lower surface area than that of the γ-Al_2O_3 support (132.03 versus 139.71 m^2/g), and the introduction of Ce decreased the surface area and total pore volume; however, the mean pore size of the catalyst increased compared with that of the γ-Al_2O_3 carrier. Fortunately, the surface area, total pore volume, and average pore size of the 3%CeO_2/γ-Al_2O_3 sample were much higher than those of CeO_2 sample.

N_2 adsorption-desorption isotherms for the γ-Al_2O_3, CeO_2, and 3%CeO_2/γ-Al_2O_3 catalyst samples are shown in Fig. 3. All the samples presented with mesoporous

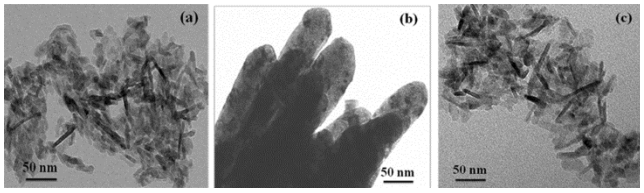

Fig. 2 — TEM image of catalyst samples: (a) γ-Al_2O_3; (b) CeO_2; (c) CeO_2/γ-Al_2O_3.

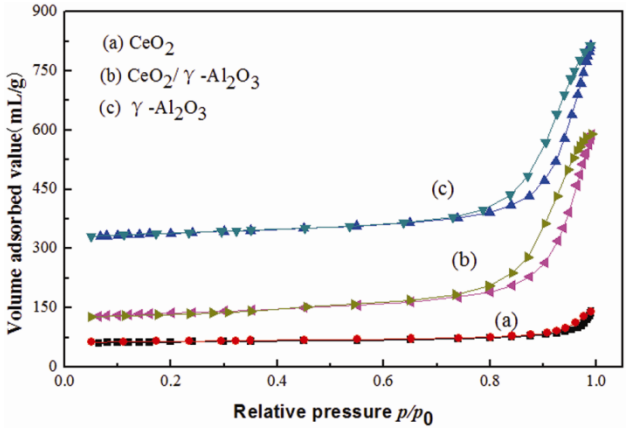

Fig. 3 — N_2 adsorption-desorption isotherms of catalyst samples.

Table 1 — Textural property of the catalyst samples.

Sample	S_{BET}/ (m^2/g)	V/(cm^3/g)	d_p/(nm)
CeO_2	46.68	0.12	10.32
γ-Al_2O_3	139.71	0.75	22.09
CeO_2/ γ-Al_2O_3	132.03	0.74	22.54

characteristics. Additionally, hysteresis loops were present in the isotherms, which were attributed to non-uniform pore size, shape and capillary condensation phenomena. The hysteresis loops of γ-Al_2O_3 were the most prominent, and the hysteresis loops of CeO_2 were less obvious. A sharp inflection point related to the rapid uptake of the adsorbate gas was noticed at relative pressures (P/P_0) of 0.75-1.0, which was related to the mesoporous nature of the interstitial pores.

A larger hysteresis loop typically indicates better adsorption properties. Hence, the degree of adsorbate uptake was higher for the CeO_2/γ-Al_2O_3 sample, while the adsorption capacity of the CeO_2 sample was relatively low owing to its low surface area. The adsorption degree of γ-Al_2O_3 sample was the best, which was consistent with the specific surface area analysis results.

XPS spectrum analysis

The elemental valence changes of CeO_2/γ-Al_2O_3 were analyzed by XPS (X-ray photoelectron spectroscopy), and the results are shown in Fig. 4. It contains C, Ce, O and Al four kinds of elements in the CeO_2/γ-Al_2O_3 catalyst (Fig. 4(a)), C comes from hydrocarbons in the air. The characteristic peak Al 2p can be observed at 73.88 eV, indicating that Al_2O_3 did not react with CeO_2. (Fig. 4(b)). It can be seen from Fig. 4(c) that the O 1s peak is asymmetric, which indicates that different types of oxygen exist on the catalyst surface. There may exist two types of oxygen on the surface of CeO_2/γ-Al_2O_3 catalyst, the characteristic lattice oxygen and chemisorbed oxygen. The addition of CeO_2 implies the binding energy of O 1s peak from 529.9 to 531.08 eV, and this shows the existence of oxygen on the catalyst surface had been affected by CeO_2. The characteristic peaks of Ce 3d XPS pattern are shown in Fig 4(d). Ce(III) can be seen at the binding energy of 884.14 eV, 904.36 eV, 919.08 eV, and Ce(IV) peaks can be observed at the binding energy of 883.98 eV, 901.38 eV, 902.58 eV. This implies that there exits exchange of Ce^{3+} and Ce^{4+} in the CeO_2/γ-Al_2O_3 catalyst. As a 4f transition

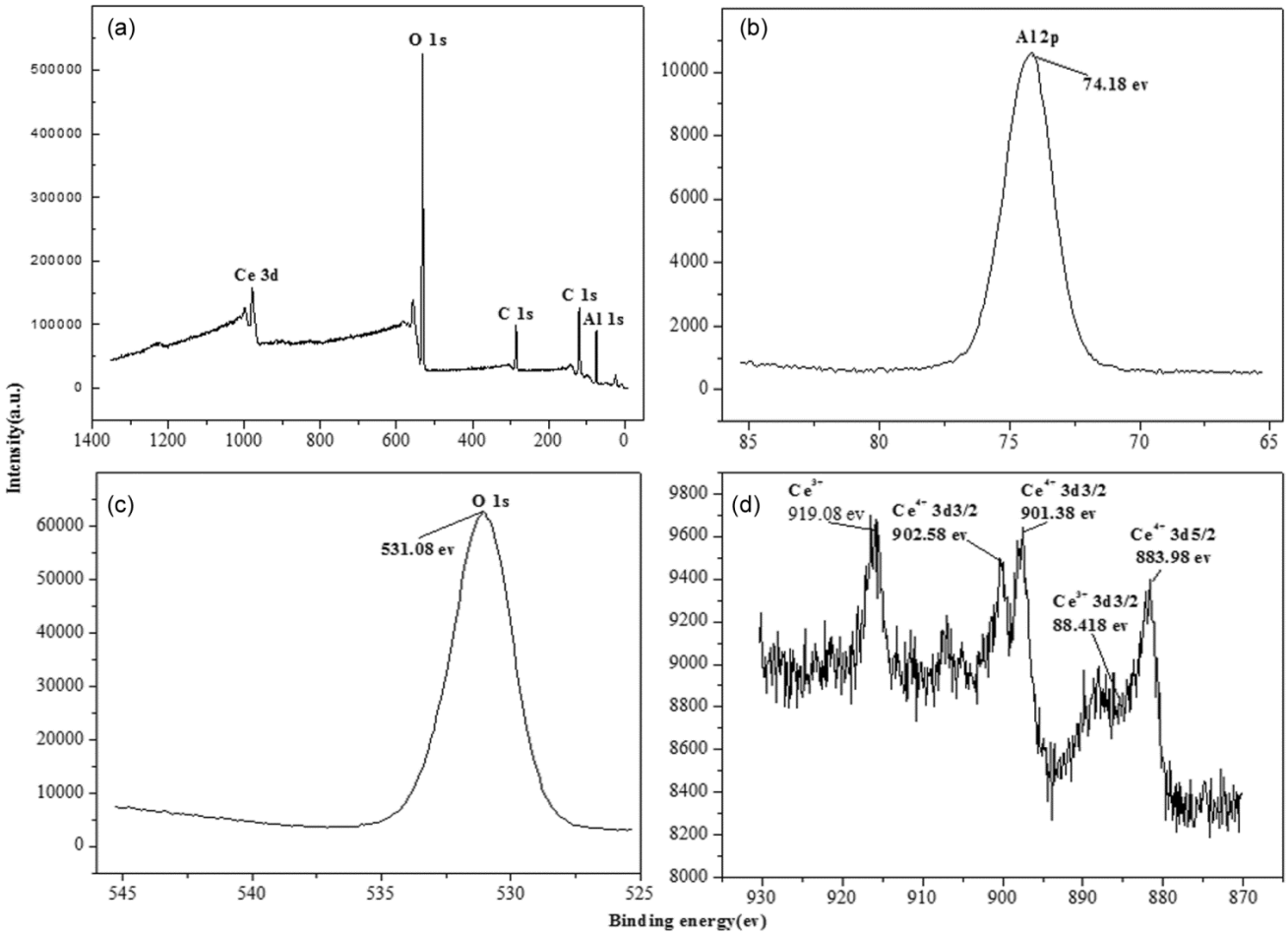

Fig. 4 — XPS spectrum of CeO_2/γ-Al_2O_3 sample

metal, Ce is excited and then emits 3d electrons. Additionally, it will also cause multiple electricity excitation as ligand O(2p) translates electrons to Ce(4f) , due to the effect of interaction between the spin orbits on the binding energy(3d3/2 and 3d5/2).

Catalytic degradation performance analysis

Figures 5-7 shows the time dependence of the methylene blue removal efficiency under different conditions. The methylene blue removal efficiencies by different catalyst samples are shown in Fig. 5 for a degradation process with a catalyst concentration of 100 mg/L at solution *p*H=10.0. The 3% CeO_2/γ-Al_2O_3 catalyst showed the best catalytic activity during the catalytic degradation process. The degradation of methylene blue was almost complete at 60 min for 3% CeO_2/γ-Al_2O_3. The removal efficiency of methylene blue by 3% CeO_2/γ-Al_2O_3 achieved a maximum value of 98.36% at 80 min, which represents an increase of 5.0% and 11.9%, compared with the efficiencies of CeO_2 and γ-Al_2O_3, respectively. The high performance was attributed to the structural and textural properties of the CeO_2/γ-Al_2O_3 catalyst owing to synergistic effects between CeO_2 and γ-Al_2O_3. We note that the catalytic degradation rate first increased and then decreased with increasing CeO_2 content in γ-Al_2O_3. The optimum mole ratio of CeO_2 to γ-Al_2O_3 was 0.03.

The effects of the amounts of catalyst on the degradation efficiency are shown in Fig. 6, with the degradation solution maintained at *p*H 10.0 and the use of the $3\%CeO_2/\gamma$-Al_2O_3 catalyst. Fig. 6 shows that the catalytic degradation rate at first increased and then decreases as the amount of catalyst was increased. Thus, the optimum catalyst amount was 100 mg/L. The degradation rate of methylene blue was 98.36% when the catalytic degradation time was 80 min. The catalytic activity first promoted because of catalytic active sites increased with increasing the amount of catalyst. Then the catalytic activity decreased might be attributed to decreased conversion efficiency of light energy owing to light-shielding and scattering effects[17]. Yu et al has found that addition of too much catalyst, the speed of •OH radical species generated is much faster than the speed of free radicals to decompose dye molecules and more free radicals are consumed by themselves, resulting in a decrease in degradation efficiency [18].

Our experimental results indicate that the catalytic reaction of methylene blue can be performed under alkaline conditions. Fig. 7 shows the effects of

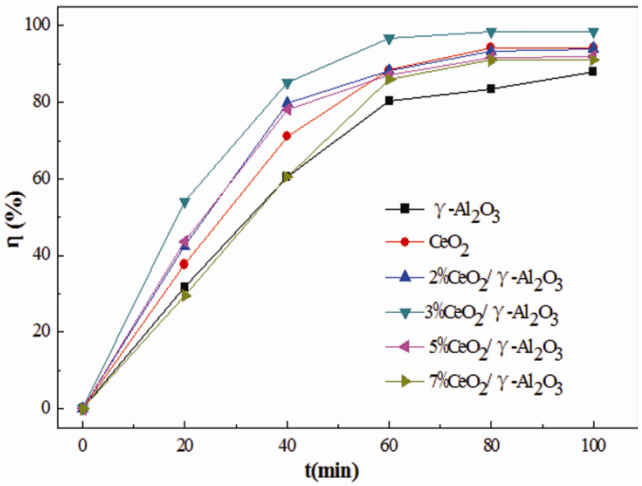

Fig. 5 — Degradation results for different catalyst samples.

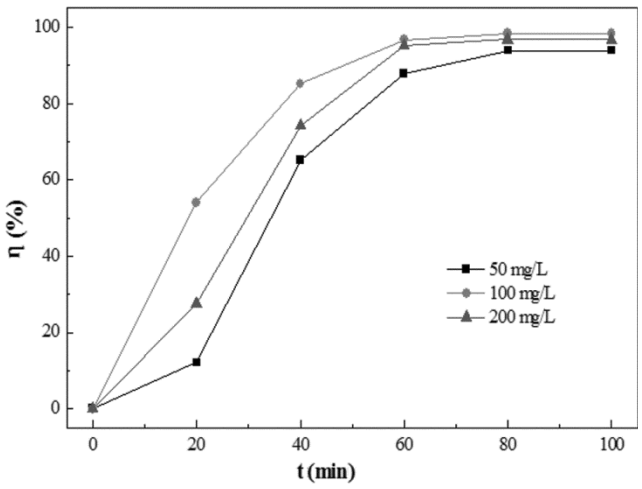

Fig. 6 — Degradation results of CeO_2/γ-Al_2O_3 catalyst with various catalyst amounts.

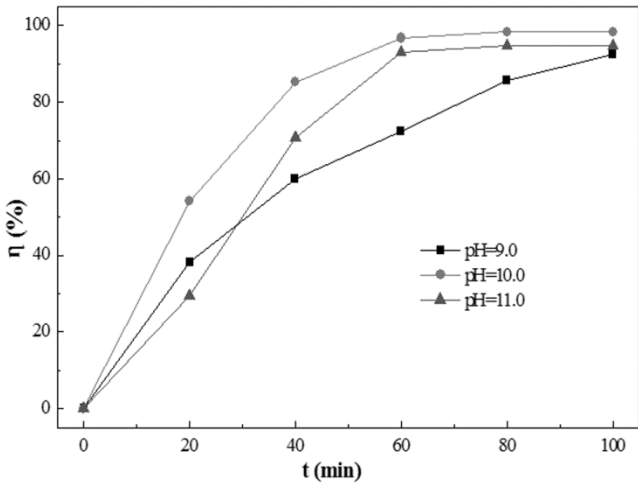

Fig. 7 — Degradation results in solutions of different pH.

solution pH on the degradation efficiency. The optimal catalytic degradation efficiency was achieved in a solution at *p*H 10.0. Under illumination •OH radicals are produced by oxidation of holes in the $CeO_2/\gamma\text{-}Al_2O_3$ composite oxides for Ce^{4+}/Ce^{3+} transformation and H_2O or OH^- in solution[19,20]. Then the •OH reacts with methylene blue to generate CO_2 and H_2O small molecules. The oxidation ability of •OH is strong in alkali solutions; which thus contributes to a higher methylene blue degradation rate. When the pH of the solution was high, more OH^- is present and more •OH is generated. However, when the solution has a high concentration of •OH radicals, the •OH can react with H_2O_2 to form O_2, which decreases the methylene blue degradation rate [21]. Therefore, the degradation rate of methylene blue was the fastest when the solution *p*H was 10.0.

NH_3-TPD result analysis

The acidities of the CeO_2 and $CeO_2/\gamma\text{-}Al_2O_3$ catalysts were characterized by NH_3-TPD, and the results were shown in Fig. 8. There were two peaks of CeO_2 catalyst in the process of adsorption NH_3, and the peak was broader at about 235□ than the peak at 90°C. Obviously the peaks of $CeO_2/\gamma\text{-}Al_2O_3$ catalyst were broader and moved to high temperature than those of CeO_2 catalyst, indicating the surface acid of the $CeO_2/\gamma\text{-}Al_2O_3$ catalyst with wider distribution. Therefore the peak area of desorption peak of $CeO_2/\gamma\text{-}Al_2O_3$ catalyst was much larger than that of CeO_2 catalyst showed that the number of surface acid sites was much more than that of CeO_2 catalyst. This was also one of the reasons for its high methylene blue degradation efficiency.

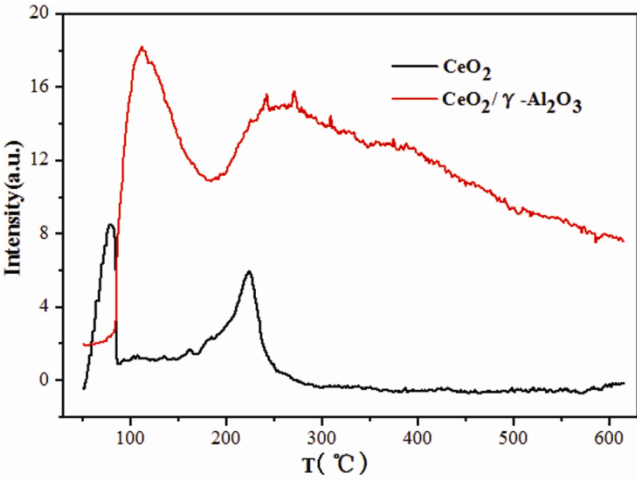

Fig. 8 — NH_3-TPD patterns of the catalyst samples.

Degradation mechanism analysis

The treatment efficiencies of the $\gamma\text{-}Al_2O_3$, CeO_2, and $CeO_2/\gamma\text{-}Al_2O_3$ catalysts in the absence of H_2O_2 were also studied. Only 30.5% degradation efficiency was achieved within 100 min with the use of $\gamma\text{-}Al_2O_3$, 35.8% degradation efficiency was achieved by the CeO_2 catalyst, and 51.2% degradation efficiency was achieved by the $CeO_2/\gamma\text{-}Al_2O_3$ catalyst. These results suggest that the degradation of the dye occurred through catalytic oxidation rather than adsorption, which can be attributed to the interactions H_2O_2, CeO_2 and $\gamma\text{-}Al_2O_3$. Small $CeO_2/\gamma\text{-}Al_2O_3$ particles with a good dispersion of CeO_2 were achieved and CeO_2 loading on the $\gamma\text{-}Al_2O_3$ increased the number of effective active sites, which helped to generate more •OH. The high content of CeO_2 promoted the content of $Ce(IV)\cdot H_2O_2$ on the surface of $CeO_2/\gamma\text{-}Al_2O_3$ catalyst, thereby improving the redox properties of the composite catalysts. There are reports that CeO_2 can act as a $\bullet OH(O_2\bullet^-)$ promoter for $CeO_2/\gamma\text{-}Al_2O_3$ catalysts [22,23]. Therefore, the catalytic activity of the $CeO_2/\gamma\text{-}Al_2O_3$ catalyst was higher than those of the $\gamma\text{-}Al_2O_3$ and CeO_2 catalysts in the degradation process. The reaction mechanism involved free radical species and is proposed as the following equations:

$$Ce(IV) + H_2O_2 \rightarrow Ce(IV)\cdot H_2O_2 \quad \ldots (1)$$

$$Ce(IV)\cdot H_2O_2 \rightarrow Ce(\text{Ⅲ}) + HO_2\bullet + H^+ \quad \ldots (2)$$

$$Ce(\square) + H_2O_2 \rightarrow Ce(IV) + \bullet OH + OH^- \quad \ldots (3)$$

$$HO_2\bullet \rightarrow H^+ + O_2\bullet^- \quad \ldots (4)$$

$$\bullet OH + \text{Methylene blue (adsorbed)} \rightarrow CO_2 + H_2O + \ldots (5)$$

$$O_2\bullet^- + \text{Methylene blue (adsorbed)} \rightarrow CO_2 + H_2O + \ldots (6)$$

The degradation proceeds by an adsorption-oxidation-desorption process. Reaction (1) occurs on the catalyst surface of CeO_2 and is a fast reaction, and reactions (2) - (4) are the key steps to produce •OH and $O_2\bullet^-$, increasing the chemisorbed oxygen content on the surface of the catalysts expedites reactions (4) to produce •OH. The produced free radical species (•OH, $O_2\bullet^-$) have high oxidative ability to decompose the adsorbed methylene blue molecules to CO_2, H_2O, or other small molecules, reaction (5) and (6). The produced small molecules from the organic dye degradation can quickly depart from the catalyst surface by desorption and the catalyst is thus recovered. Yu has reported that •OH radicals, which are generated directly from H_2O_2 with sufficient quantity by catalyzing H_2O_2 under the role of catalyst, have a powerful ability to oxidize and decompose organic dye [24].

To analyze the change of the •OH concentration in the catalytic degradation process, a salicylic acid fluorescence detection method was used to capture •OH radicals[25]. These results are shown in Fig. 9. A large amount of •OH was produced when CeO_2/γ-Al_2O_3 was used as the catalytic oxidizer and oxidation by •OH was the main degradation pathway. The •OH concentration decreased considerably when the oxidation reaction was performed for 60 min. This result was attributed to salicylic acid being oxidized by remaining H_2O_2 in the reaction system resulting in a weakening of the fluorescence intensity.

Kinetic analysis of the degradation process

To study the kinetic factors of the catalytic degradation process of methylene blue, γ-Al_2O_3, CeO_2, and CeO_2/γ-Al_2O_3 catalyst samples were used. According to the least square method for the linear fitting results, a quasi-first orders kinetic equation (7) was established. The kinetic model for multiphase catalytic reactions is accordance with the L-H kinetic equation [26, 27]:

$$r = -\frac{dc_t}{dt} = \frac{kK_{dye}c_t}{1+K_{dye}c_0} = k_{app}c_t \quad \ldots (7)$$

Where c_0 and c_t are the initial and final concentrations of methylene blue (mg/L), K_{dye} is the L-Hadsorption equilibrium constant (L/mg), k is the apparent rate constant [mg/ (L·min)], k_{app} is a quasi-rate constant.

Linear fits of ln (c_0/c_t) versus time are shown in Fig 10. The k_{app} values were calculated as 17.5×10^{-2}, 7.5×10^{-2}, and 5.0×10^{-2} for CeO_2/γ-Al_2O_3, CeO_2, and γ-Al_2O_3, respectively. The k_{app} value for the CeO_2/γ-Al_2O_3 catalyst samples was greatest, which was 1.33 and 2.5 times as large as those of CeO_2 and γ-Al_2O_3, respectively. Thus the degradation rate of the CeO_2/γ-Al_2O_3 catalyst on methylene blue was more rapid, which agreed well with the degradation results discussed above.

Conclusion

Methylene blue dye could be efficiently degraded with the use of a CeO_2/γ-Al_2O_3 catalyst. CeO_2/γ-Al_2O_3 show better catalytic activity than those of CeO_2 and γ-Al_2O_3 catalysts under the same reaction conditions. The results of the catalysts characterization and catalytic tests indicate that good dispersion of CeO_2 in the CeO_2/γ-Al_2O_3 catalyst is achieved, which contribute to a high surface area and large number of

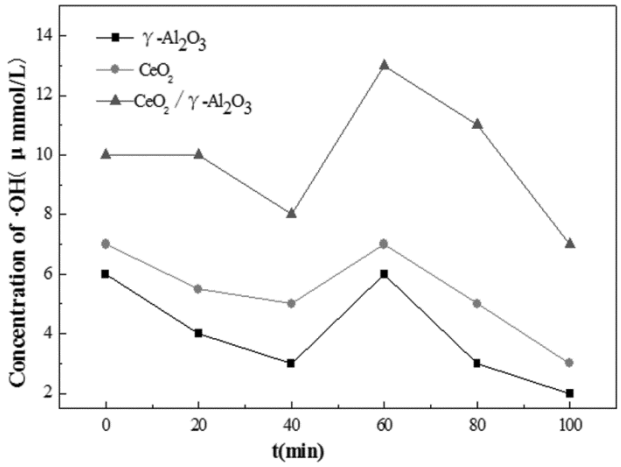

Fig. 9 — Changes of ·OH concentration in the degradation process.

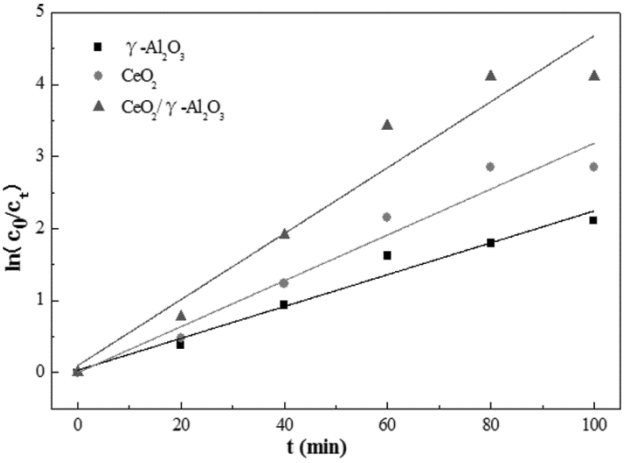

Fig. 10 — Linear fits of ln (c_0/c_t) versus time.

effective acid sites. Furthermore, synergistic effects between CeO_2 and γ-Al_2O_3 increase the content of •OH (O_2•$^-$) on the surface of CeO_2/γ-Al_2O_3 catalyst, which improve the redox properties of the composite catalyst. Kinetic analysis show that the k_{app} value of the CeO_2/γ-Al_2O_3 catalyst samples is approximately 1.33 times as high as that of CeO_2 and 2.5 times as big as that of γ-Al_2O_3. These results confirm those from our catalytic degradation tests. Thus, our mixed composite catalyst shows promising for applications to the treatment of dye wastewater.

Acknowledgements

This project was financially supported by the National Natural Science Foundation of China (No:41763008), National Science Foundation of Hunan Province (No.2018JJ2112), Natural Science Foundation of Guizhou Province ([2017]1198), and projects of "Chemical First-class Subjects" ([2018]40).

References

1 Carmen Z & Daniela S, *Conv Anal Updat*, 55 (2012) 1.
2 Sajab M S, Chia C H, Zakaria S & Khiew P S, *Bioresour Technol*, 128 (2013) 571.
3 Marrakchi F, Auta M, Khanday W A & Hameed B H, *Powder Technol,* 321 (2017) 428.
4 Liu Y & Sun D Z, *J Hazard Mater,* 143 (2007) 448.
5 Alama U, Khana A, Razaa W, Khanb A & Bahnemanncd D, *Catal Today,* 284 (2017) 169.
6 Prabha I & Lathasree S, *Mater Sci Semicond Process,* 26 (2014) 603.
7 Prabha I, Lathasree S, *J Mol Catal A,* 281 (2008) 119.
8 Machida M, Kawada T, Fujii H & Hinokuma S, *J Phys Chem C,* 119 (2015) 24932.
9 Singh P & Hegde M S, *Dalton T,* 39 (2010) 10768.
10 Jia L, Shen M, Hao J, Rao T & Wang J, *J Alloys Compd,* 454 (2008) 321.
11 Saravanakumar K, MymoonRamjan M, Suresh P & Muthuraj V, *J Alloy Compd,* 664 (2016)149.
12 Peng X J, Luan Z K & Ding J, *Mater Lett,* 59 (2005) 399.
13 Rao R, Zhang Q Y & Liu H D, *J Mol Catal A Chem,* 363 (2012) 283.
14 Phanichphant S, Nakaruk A & Channei D, *Appl Surf Sci,* 387 (2016) 214.
15 Liu Y & Sun D Z *J, Hazard. Mater,* 143 (2007) 448.
16 Neves T M, Frantz T S, Schenque E C C, Gelesky M A & Mortola V B, *Environ Technol Innov* 8 (2017) 349.
17 Wetchakun N, Chaiwichain S, Inceesungvorn B, Pingmuang K, Phanichphant S, Minett A I & Chen J, *ACS Appl Mater Interfaces,* 4 (2012) 3718.
18 Yuan C L, Li Gao, Wei L F, Fan Q Z, Shua Q, Jimmy C & Yu, *Catalysis Today,* 224 (2014) 154.
19 Choudhury B, Chetri P & Choudhury A, *RSC Adv,* 4 (2014) 4663.
20 Zheng X G, Huang S, Yang D M, Zhai H Y, You Y H, Fu X J, Yuan J H, Zhou X K, Wen J & Liu Y, *J Alloy Compd* 25 (2017) 131.
21 El Rouby W M A, Farghali A A & Hamdedein A, *Water Sci Technol* 10 (2016) 2325.
22 Gemeay A H, El-Sharkawy R G, Mansour I A & Zaki A B, *Appl Catal B,* 80 (2008) 106.
23 Souza Br S, Moreira F C, Dezotti M W C, Vilar V J P & *Boaventura* R A R, *Catal Today,* 209 (2013) 201.
24 Yu J G, Dai G P & Xiang Q J & Jaroniec M, *J Mater Chem* 21 (2011) 1049.
25 Albarrán G & Mendoza E, *Radiat Phys Chem,* 147 (2018) 27.
26 Pouretadal H R & Kadkhodaie A, *Chinese J Catal*, 31 (2010) 328.
27 Yang B, Tian Z, Zhang L, Guo Y P & Yan S Q, *J Water Process Eng,*5 (2015) 101.